

Physical Interpretation of the “Kinetic Energy Release” Effect in the Double Photoionization of H₂

T. J. Reddish,¹ J. Colgan,² P. Bolognesi,³ L. Avaldi,³ M. Gisselbrecht,⁴ M. Lavollée,⁴ M. S. Pindzola,⁵ and A. Huetz⁴

¹Department of Physics, University of Windsor, 401 Sunset Ave, Ontario, Canada, N9B 3P4

²Theoretical Division, Los Alamos National Laboratory, Los Alamos, New Mexico 87545, USA

³CNR-IMIP Area della Ricerca di Roma 1, CP 10 00016 Monterotondo Scalo, Italy

⁴CNRS-Université Paris Sud, UMR8624, LIXAM, Bat. 350, Centre d’Orsay, 91405, Orsay, France

⁵Department of Physics, Auburn University, Auburn, Alabama 36849, USA

(Received 25 January 2008; published 14 May 2008)

A physical interpretation is given for the variation with internuclear separation of the fully differential cross section for double photoionization of H₂. This effect is analyzed in a geometry where the fourbody interaction is completely probed. Excellent agreement is found between experiment and time-dependent close-coupling theory after convoluting the latter over the relevant solid angles. We show the observed variations are purely due to the ε_{Σ} component of the polarization vector ε along the molecular axis, a conclusion which is supported through calculations of the photoionization of H₂⁺.

DOI: 10.1103/PhysRevLett.100.193001

PACS numbers: 33.80.Eh, 34.10.+x

Double ionization of H₂ by a single photon results in four unbound charged particles: two protons and two electrons. That this process occurs at all is directly due to electron correlation in the initial and final states, making this process of fundamental interest. During the “Coulomb explosion”, the two bare nuclei fly apart in opposite directions on a rapid time scale (fs) compared to molecular rotation (ps). Consequently, knowing the vector momentum of the escaping protons gives the molecular alignment at the moment of double ionization, and its spherical angles θ_N , ϕ_N defined with respect to the linear polarization vector, ε . Recent developments in coincidence techniques [1,2] have enabled all four particle’s momenta to be determined experimentally, resulting in electron angular distributions within the *molecular* frame [3,4]. These fully differential cross sections (FDCSS) are the most sensitive signatures of the correlated dynamics of the escaping electron pair within this axially symmetric potential, and are strongly dependent on θ_N , in both magnitude and shape.

The purely Coulombic character of the final state potential is shown schematically in Fig. 1. This steeply repulsive curve results in the protons’ “kinetic energy release” (KER) depending on the precise value of R at the moment of double ionization. Filtering the data set reported in [4] as a function of ion energy, E_N , which is proportional to $1/R$, allows one to probe the interplay between the electronic and nuclear motion in the double photoionization (DPI) of H₂.

The only previous experimental study on so-called “KER effects” identified differences in the FDCS in the “perpendicular” plane geometry, where the reference electron is chosen to be orthogonal to ε (i.e.: $\theta_1 = 90^\circ$), the molecular axis, and the second electron [5]. The cross section is very small in this detection geometry, which is physically very specific as the mutual angle between the

electrons is fixed so freezing the electron-electron interactions. Recent theoretical work, using the exterior complex scaling (ECS) [6] and time-dependent close-coupling (TDCC) methods [7] also find some R variation in the FDCS for this geometry. However, none of these previous studies uncovered the physical origin of this phenomenon.

Here we present FDCSS in the “coplanar” geometry, where all four particles and ε all lie in the same plane. The cross section is much larger in this geometry, compared to that in the perpendicular plane; moreover both the electron-electron and electron-ion interactions are being probed.

The FDCS measurements were obtained using 100% linearly polarized light from the Elettra synchrotron in conjunction with the CIEL momentum imaging apparatus; further details are given elsewhere [2,4,8]. The photon

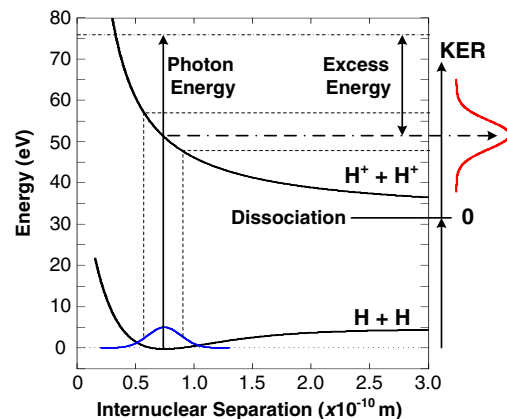


FIG. 1 (color online). Schematic potential energy diagram of the initial and final states for DPI of H₂. During double ionization the ground vibrational state is projected onto the upper repulsive curve, whose dissociation limit is at 31.67 eV, resulting in a broad range of kinetic energies for the final proton pair.

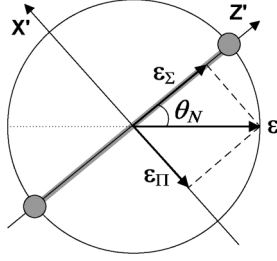


FIG. 2. Schematic diagram of the body-fixed frame ($X'Y'Z'$) showing the ε vector split into two components, along (ε_{Σ}) and perpendicular (ε_{Π}) to the molecular axis. When the molecular axis is aligned parallel and perpendicular to ε , one can obtain the pure Σ and pure Π amplitudes, respectively.

energy was 76.09 eV, ~ 25 eV above the nominal threshold at the equilibrium internuclear separation ($1.4 a_0$) and near the peak maximum of the total DPI cross section.

The observed FDCSs are compared to those obtained using the TDCC method, which has been described in detail previously [9,10]. To study the KER dependence, a TDCC calculation is performed at different values of R . A TDCC calculation is also made for each final M symmetry accessible by a single-photon transition (i.e. $M = 0, \pm 1$, where M is the total magnetic quantum number in the body frame (Fig. 2)). When constructing FDCSs, the amplitudes which result from these calculations must be added coherently, and are weighted by appropriate factors for a given molecular orientation [[10], Eq. (11)]. Thus, the total contribution to the FDCS consists of a Σ ($M = 0$) component, a Π ($M = \pm 1$) component, and cross terms arising when the total amplitude is squared to obtain the FDCS.

Convolution over experimental solid angles can easily mask or smear out the KER-dependent FDCS. An advantageous feature of momentum imaging methods is the ability to select the experimental bandwidths in the data analysis, and is completely decoupled from the data acquisition. Although ~ 1.1 million four particle coincidence events were obtained in this study [4], careful attention was still needed in choosing the critical variables over which one can convolute large ranges without compromising the direct observation of KER effects. To compare with experiment, the TDCC FDCSs are also convoluted, by performing calculations for a detailed grid of angles and energies over the range of experimental bandwidths, and then appropriately averaging the results. We also examined the TDCC FDCS as a function of the various bandwidths to determine which variables are most sensitive to the convolution procedure. It was found that θ_N was the most critical variable to minimize, and that the other variables were insensitive to convolution, even over fairly large ranges. Hence we selected $\Delta\theta_N = \pm 10^\circ$ but with large values of the other bandwidths and with $E_1 = E_2 = 12.5 \pm 10$ eV, in both the experimental measurements and in the TDCC convoluted calculations.

The FDCSs at $\theta_1 = 90^\circ$ for $\theta_N = 90$ and 0° , allowing one to obtain experimentally the Π and Σ amplitudes,

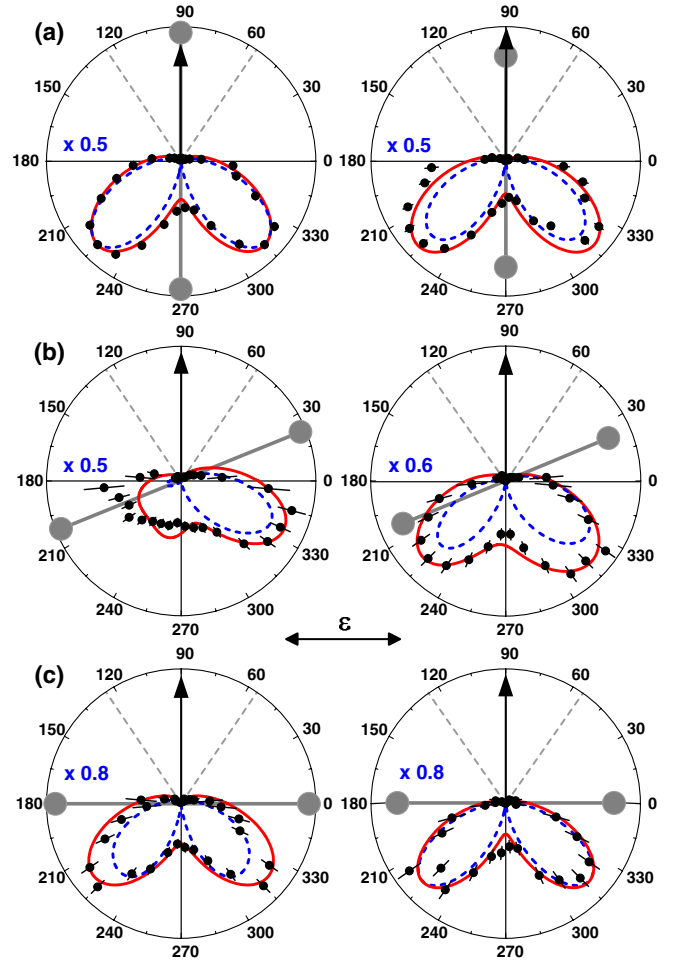


FIG. 3 (color online). H_2 FDCSs in the “coplanar” geometry for three “in plane” molecular orientations, $\theta_N =$ (a) 90° , (b) 20° , and (c) 0° , all with the first electron at $\theta_1 = 90^\circ$ and for $E_1 = E_2 = 12.5 \pm 10$ eV. Two KER values, (a),(b) 16.5 (left) and 23.5 eV (right), and (c) 16 (left) and 24 eV (right), corresponding to approximately $R = 1.6, 1.2 a_0$, respectively, are shown for each θ_N angle. The angular step in θ_2 is 10° . The dotted lines indicate a dead sector, symmetric with respect to the vertical axis, for the detection of the second electron. The bandwidths are: $\Delta E_{\text{KER}} = \pm 2$ eV (a),(b), ± 4 eV (c); $\Delta\theta_N = \pm 10^\circ$; $\Delta\theta_1 = \pm 20^\circ$; $\Delta\phi_{12} = \pm 45^\circ$; $\Delta\phi_{1N} = \pm 60^\circ$ [not relevant in (c)]. The experimental data are arbitrarily normalized to the TDCC results convoluted over the experimental bandwidths (solid); unaveraged TDCC results for the stated (θ_1, θ_N) values (dashed) have the scaling factors indicated.

respectively, are shown in Figs. 3(a) and 3(c) for two R values. The results of TDCC calculations at a fixed R are also shown, both for the stated (θ_1, θ_N) values and convoluted over the experimental bandwidths. Integration over R as a continuous variable is not performed in the TDCC averaging, thus preventing a precise comparison with the experimental data on an absolute scale. Convolution over the other dynamical variables nevertheless allows for a direct comparison of the experimental and theoretical FDCS shapes. Note that the strict quantum mechanical node for “back-to-back” emission of the two electrons

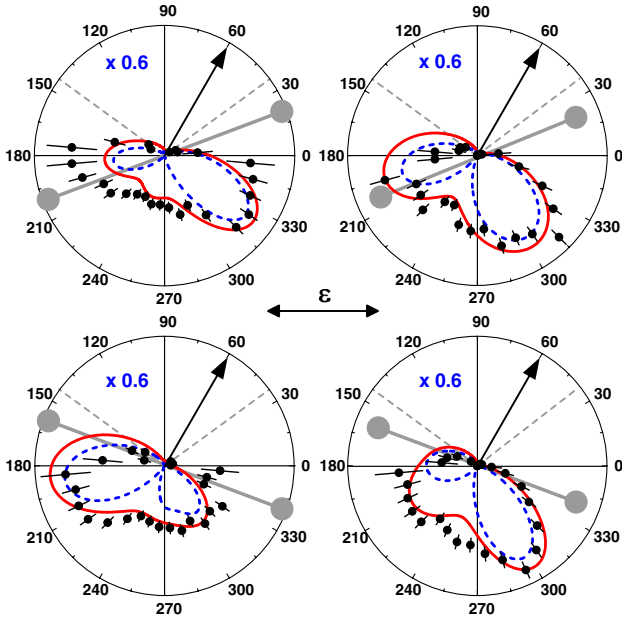


FIG. 4 (color online). As in Fig. 3(b), but for molecular orientations $\theta_N = 20^\circ, 160^\circ$; all with $\theta_1 = 60^\circ$.

with $E_1 = E_2$ predicted by the DPI selection rules [11] appears in the calculations (dashed curves) but is smoothed out in the convoluted calculations and in the data.

Figure 3(a) shows that there is virtually no difference in FDCS as a function of R in the Π orientation. There is, however, a small difference in the FDCS shape for the Σ orientation [Fig. 3(c)] that, in the experimental data, is most evident in the vicinity of the ε direction. At intermediate molecular orientations and without KER selection (See [4], Fig. 1), the two lobes have asymmetric amplitudes with the most intense lobe lying in the “3rd quadrant” in these coplanar geometry polar plots. Figure 3(b) shows that when $\theta_N \sim 20^\circ$ there is a dramatic change in the FDCS with R . At large R , virtually all the yield is in the 4th quadrant; only convolution over the solid angles provides intensity in the 3rd quadrant. The dashed curves indicate that such a spectacular evolution with R exists at exact equal energy sharing and survives when almost all electron energy sharings are included (solid curves).

Figure 4 shows the FDCS variation with R at $\theta_1 = 60^\circ$ for $\theta_N = 20$ and 160° . Again one observes the hitherto unexpected sensitivity of the coplanar FDCS to internuclear separation. There is a rapidly evolving FDCS for both values of θ_N , which have excellent agreement in shape with the convoluted TDCC results.

Figure 5 shows the variation in FDCS at $\theta_1 = 0^\circ$ for fixed large R with $\theta_N = 40$ and 20° . When $\theta_1 = 0^\circ$ and $\theta_N = 90^\circ$ one expects a symmetric lobe structure due to symmetry (see Fig. 2 of [4]). As θ_N departs from 90° towards 0° , and without KER selection, the lobe in the 2nd quadrant reduces dramatically in intensity and then steadily increases until the FDCS has symmetric lobes for $\theta_N = 0^\circ$; the $\theta_N = 40^\circ$ FDCS in Fig. 5 is illustrative of

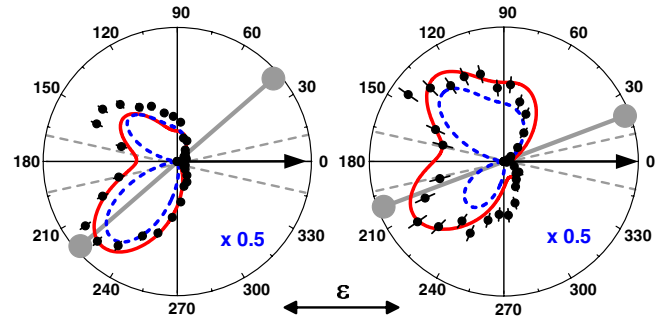


FIG. 5 (color online). As in Fig. 3(c), but for molecular orientations $\theta_N = 40^\circ$ and 20° ; all with $\theta_1 = 0^\circ$ and $R = 1.6 a_0$. ($\Delta\phi_{12}$ and $\Delta\phi_{1N}$ are not relevant, $\Delta\phi_{2N} = \pm 60^\circ$).

that behavior at an intermediate θ_N value. However, as θ_N rotates from 40° to 20° , most of the FDCS yield changes to the 2nd quadrant for large R , but not for small R (not shown).

Is there a simple physical explanation for the spectacular R dependence reported in Figs. 3(b), 4, and 5? Why is $\theta_N \sim 20^\circ$ so critical to observe these KER effects?

As already mentioned and illustrated in Fig. 2, the FDCS is the coherent sum of Π and Σ components. In the TDCC FDCS, we extract the Σ and Π components, and cross term contributions for the first time. Such information reveals the relative importance of each term. At $\theta_N = 20^\circ$, shown in Fig. 6, both components make significant contributions to the FDCS and *only* the Σ component displays an appreciable dependence on R . Moreover, changes in sign (and shape) of the cross term with R results in constructive and destructive interference between the two components, respectively, and “amplifies” the small changes with R of the pure Σ component. Hence only at $\theta_N \sim 20^\circ$ (or equivalently, 160°) are spectacular KER effects to be observed.

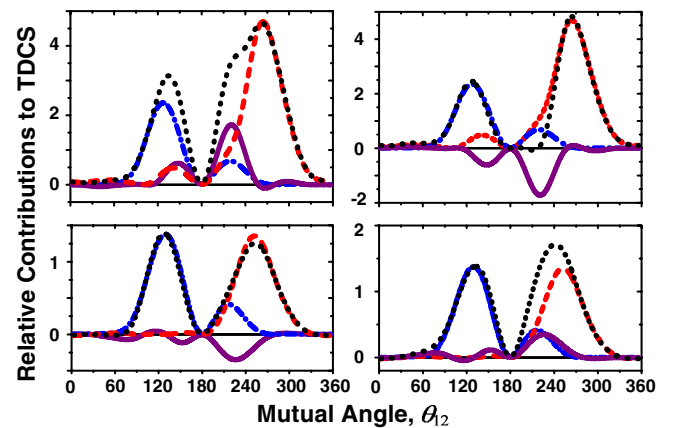


FIG. 6 (color online). The relative contributions to the TDCC FDCS (dot) from the pure Π (dash-dot) and Σ (dash) contributions, and their cross term (solid), for (θ_1, θ_N) values of $(20^\circ, 160^\circ)$ left and $(60^\circ, 20^\circ)$ right, and for $R = 1.6$ (upper) and 1.2 (lower). At these (θ_1, θ_N) values the peaks at $\theta_{12} \sim 130^\circ$ and $\sim 250^\circ$ in the total FDCS are primarily due to the Π and Σ contributions, respectively; see text for discussion.

Interestingly, the cross terms for the θ_1 and θ_N angles shown in Fig. 6 differ from each other by a simple sign change for corresponding R values. This observation can be understood within the body-fixed (BF) frame (see Fig. 2). In this frame, the FDCS = $|A_\Sigma + A_\Pi|^2$, where A_Σ and A_Π are the two weighted amplitudes. In rotating both the molecule and the electrons by $2\theta_N$, thus changing $\theta_N \rightarrow -\theta_N$, the BF ε_Σ component is unchanged, whereas the $\varepsilon_\Pi \rightarrow -\varepsilon_\Pi$, resulting in $\text{FDCS} \rightarrow |A_\Sigma - A_\Pi|^2$. The (θ_1, θ_N) angles of the right and left columns of Fig. 6 are related by such a rotation (of 40°), hence the sign change for each R value.

Now that the magnification of the KER effect at $\theta_N \sim 20^\circ$ or 160° is well understood as an interference effect, a new question arises. Why is, exclusively, the angular dependence of the Σ amplitude sensitive to R ? A related but different question is: why is Π the dominant amplitude? A recent ECS study [6] revealed an unexpected feature, namely, that the magnitude of the Π amplitude decreases monotonically with R , whereas the Σ amplitude has a shallow minimum near the equilibrium separation. This behavior has also been found in the present TDCC results. Furthermore, the dominance of the Π amplitude results in a negative ion asymmetry parameter β_N that also varies with R due to the differences in the R dependencies of the Σ and Π amplitudes. The observed β_N value of -0.75 ± 0.1 [4] at this photon energy is in excellent agreement with the R -averaged TDCC β_N value of -0.73 .

To investigate these questions we first recognize that $M = 0$ (Σ) and $M = \pm 1$ (Π) electronic states have different spatial distributions in the $(X'Y'Z')$ BF of Fig. 2. This leads us to revisit a simpler but instructive process, the photoionization of H_2^+ . As there is a complete absence of electron-electron correlation in H_2^+ , this allows one to see purely the effects of the localization of the continuum electron in the nonspherical potential. Over 50 years ago, analytical studies using confocal elliptical coordinates investigated the π and σ amplitudes in the photoionization cross section as a function of R for a photoelectron energy of 0 eV [12]. The p partial wave contribution to the π amplitude is dominant and decreases monotonically with R from 0 to $4 a_0$. In contrast, the p partial wave contribution to the σ amplitude has a minimum at equilibrium separation, $R = 2 a_0$, and at higher values of R is strongly mixed with the f partial wave contribution. As a consequence of these very different behaviors, the π amplitude dominates (which also results in a negative β_N for this process) but has an angular distribution, with a maximum at right angles with the internuclear axis, almost independent of R , whereas the σ amplitude is smaller but exhibits a spectacular KER effect in its angular distribution, which is maximum along the internuclear axis. We find essentially the same behavior using a time-dependent approach [13,14], which constructs initial and final states of H_2^+ on a grid, and which can be used to investigate the resulting

photoelectron angular distributions. The KER effects found near threshold are also found at higher photoelectron energies [15].

The DPI of H_2 is much more complex than photoionization of H_2^+ , as the l_1, l_2 partial wave expansions of the Π and Σ amplitudes are determined not only by the nonspherical potential, but also by electron correlation. However by limiting the number of angular momenta retained in the TDCC calculations, we find that low l_1, l_2 dominate the Π amplitude, whereas larger l_1, l_2 are necessary for convergence of the Σ amplitude. This gives confidence in the analogy between H_2^+ and H_2 , and in the conclusion that the main R -dependent trends of the Π and Σ amplitudes observed in H_2 double ionization are due to electron-ion rather than electron-electron interactions. The relative strength of the higher partial waves in the Σ amplitude accounts for the observation that the most significant KER effects only occur at large R (see Figs. 3–5). Finally, we note that the Σ electronic states, which are sensitive to variations in R , in general lie near the internuclear axis, while the Π states, which are relatively insensitive to changes in R , are more concentrated in the plane between the nuclei.

We would like to thank the staff at Elettra and the Gas Phase beam line team for their invaluable assistance, and EU, NSERC and UoW for their financial support. Some of this work was performed under the auspices of the U.S. DOE through Los Alamos National Laboratory (LANL) and through NSF and DOE grants to Auburn University. Computational work was carried out at NERSC in Oakland, CA, the NCCS in Oak Ridge, TN, and through LANL Institutional Computing Resources.

-
- [1] R. Dörner *et al.*, Phys. Rep. **330**, 95 (2000).
 - [2] M. Gisselbrecht *et al.*, Rev. Sci. Instrum. **76**, 013105 (2005).
 - [3] Th. Weber *et al.*, Phys. Rev. Lett. **92**, 163001 (2004).
 - [4] M. Gisselbrecht *et al.*, Phys. Rev. Lett. **96**, 153002 (2006).
 - [5] T. Weber *et al.*, Nature (London) **431**, 437 (2004); **443**, 1014 (2006).
 - [6] D. A. Horner *et al.*, Phys. Rev. Lett. **98**, 073001 (2007).
 - [7] J. Colgan *et al.*, J. Phys. B **40**, 4391 (2007).
 - [8] M. Gisselbrecht *et al.*, J. Phys.: Conf. Ser. **88**, 012006 (2007).
 - [9] J. Colgan, M. S. Pindzola, and F. Robicheaux, J. Phys. B **37**, L377 (2004).
 - [10] J. Colgan, M. S. Pindzola, and F. Robicheaux, Phys. Rev. Lett. **98**, 153001 (2007).
 - [11] M. Walter and J. S. Briggs, Phys. Rev. Lett. **85**, 1630 (2000).
 - [12] D. R. Bates, U. Öpik, and G. Poots, Proc. Phys. Soc. London Sect. A **66**, 1113 (1953).
 - [13] J. Colgan *et al.*, Phys. Rev. A **68**, 063413 (2003).
 - [14] M. Foster *et al.*, Phys. Rev. A **75**, 062707 (2007).
 - [15] J. Colgan *et al.*, J. Phys. B **41**, 085202 (2008).